HSPI The Open Access Publisher

IJPRA ISSN 2766-2748 INTERNATIONAL JOURNAL OF PHYSICS RESEARCH AND APPLICATIONS

Research Article

Superior Gas Sensing Properties Achieved through La-Doping in $BiFeO_3$: The Case of $Bi_{0.75}La_{0.25}FeO_3$

Avinash R Gaikwad[1,2], Ajinkya G Bagde[3] and Ravi S Kawale[4]*

[1]Department of Physics, N.E.S. Science College, Nanded, MS 431605, India
[2]Department of Physics, Vivekanand College, Kolhapur, MS 416003, India
[3]Shri Sant Gadge Maharaj College, Loha, Dist. Nanded, MS 431708, India
[4]Dnyanopasak Shikshan Mandal's Arts, Commerce and Science College, Jintur, Dist. Parbhani, MS 431509, India

More Information

***Corresponding author:** Ravi S Kawale, Dnyanopasak Shikshan Mandal's Arts, Commerce and Science College, Jintur, District, Parbhani, MS 431509, India, Email: ravi.kawale1972@gmail.com

Submitted: March 24, 2026
Accepted: April 02, 2026
Published: April 03, 2026

Citation: Gaikwad AR, Bagde AG, Kawale RS. Superior Gas Sensing Properties Achieved through La-Doping in $BiFeO_3$: The Case of $Bi_{0.75}La_{0.25}FeO_3$. Int J Phys Res Appl. 2026; 9(3): 065-070. Available from: https://dx.doi.org/10.29328/journal.ijpra.1001148

Keywords: Lanthanum-doped bismuth ferrite; Sol-gel method; Gas sensors

Abstract

Lanthanum-substituted bismuth ferrite ($Bi_{0.75}La_{0.25}FeO_3$) nanoscale perovskite powders were synthesized using a sol–gel auto-combustion technique, with citric acid employed as a fuel agent. The synthesized materials were systematically characterized to examine their structural, morphological, and gas-sensing properties. X-ray diffraction analysis confirmed the formation of a well-defined rhombohedrally perovskite phase. Further insights into bonding characteristics and surface morphology were obtained through infrared spectroscopy and field-emission scanning electron microscopy. The gas-sensing performance was evaluated for NO_2, CO_2, Ethanol, and NH_3 over a concentration range of 5-100 ppm, with an optimal operating temperature of 200 °C. The results indicate that lanthanum incorporation significantly influences the structural features and enhances the sensing response with a response time of 11s and a recovery time of 64s. Overall, the study highlights the suitability of La-doped bismuth ferrite nanopowders as promising candidates for efficient gas-sensing applications, demonstrating a strong relationship between structural modifications and sensor performance.

Introduction

The detection of hazardous and combustible gases has become increasingly important due to rising environmental concerns, industrial safety requirements, and domestic risk management. Among various sensing materials, semiconducting metal oxides have attracted considerable attention because of their high sensitivity, stability, and cost-effectiveness. In particular, perovskite-type oxides are promising candidates for gas-sensing applications owing to their tunable electrical and structural properties. Bismuth ferrite ($BiFeO_3$) is a well-known multiferroic perovskite material that exhibits a narrow band gap (~2.2-2.6 eV), good chemical stability, and excellent redox activity, making it suitable for gas sensor applications. Its sensing mechanism is primarily governed by surface adsorption and charge transfer processes between the target gas and adsorbed oxygen species. However, pristine $BiFeO_3$ often suffers from limitations such as low selectivity, moderate sensitivity, and high operating temperature, which restrict its practical applicability [1]. To overcome these limitations, various modification strategies such as doping and composite formation have been explored. Elemental doping at the A-site or B-site of the perovskite lattice can significantly alter the electrical conductivity, grain size, oxygen vacancy concentration, and surface reactivity of $BiFeO_3$. For instance, doping with elements such as barium or indium has been shown to enhance gas-sensing performance by reducing particle size and increasing surface area, thereby improving gas adsorption and sensitivity [2,3].

Similarly, the incorporation of graphene oxide into $BiFeO_3$ matrices has demonstrated improved response and faster recovery characteristics due to enhanced charge transport pathways [1]. Among various dopants, lanthanum (La^{3+}) has attracted particular interest due to its ability to substitute Bi^{3+} ions effectively without significantly disturbing the

perovskite structure. Lanthanum doping can induce lattice distortion, suppress impurity phases, and enhance oxygen vacancy concentration, which plays a crucial role in gas-sensing mechanisms. Recent studies have shown that La-doped bismuth-based oxides exhibit improved selectivity, stability, and sensing response due to enhanced surface adsorption and catalytic activity [4]. The introduction of La also contributes to better crystallinity and controlled grain growth, which are essential factors for improving sensor performance. Furthermore, synthesis techniques play a critical role in determining the structural and morphological properties of sensing materials. The sol-gel auto-combustion method is widely employed due to its simplicity, low cost, and ability to produce homogeneous nanosized powders with high surface area. The use of organic fuels such as citric acid facilitates controlled combustion, resulting in fine particles and improved porosity, which are advantageous for gas sensing [5].

In this context, the present study focuses on the synthesis of lanthanum-doped bismuth ferrite ($Bi_{0.75}La_{0.25}FeO_3$) nanopowders using a sol-gel auto-combustion approach. The structural, morphological, and gas-sensing properties are systematically investigated to understand the influence of La incorporation. Special emphasis is given to the detection of NH_3 gas, which is widely used in domestic and industrial applications but poses significant safety risks due to its flammability. The study aims to establish a clear correlation between structural modification induced by lanthanum doping and the resulting enhancement in gas-sensing performance.

Experimental section

Chemicals and materials

Bismuth nitrate pentahydrate ($Bi(NO_3)_3{\cdot}5H_2O$), lanthanum nitrate hexahydrate ($La(NO_3)_3{\cdot}6H_3O$), ferric nitrate nonahydrate ($Fe(NO_3)_3{\cdot}9H_2O$), citric acid ($C_6H_8O_7 \cdot H_2O$), and doubly distilled water (DDW) as solvent (all reagents analytical grade and purchased from Sigma Aldrich). All chemicals were used as received without further purification.

Synthesis of lanthanum-doped bismuth ferrite ($Bi_{0.75}La_{0.25}FeO_3$).

The Lanthanum-doped bismuth ferrite ($Bi_{0.75}La_{0.25}FeO_3$) nanopowders were synthesized using a sol-gel auto-combustion method in Figure 1, which is widely employed for the preparation of homogeneous and nanoscale perovskite materials due to its simplicity and effectiveness [6,7]. In this process, precursor solutions were prepared separately and then combined to obtain a uniform reaction mixture. Initially, citric acid was dissolved in distilled water, maintaining its molar concentration equal to the total molar amount of metal ions (Bi^{3+}, La^{3+}, and Fe^{3+}). Citric acid acted as a chelating agent, ensuring uniform mixing of metal ions and preventing phase segregation during synthesis [8]. Bismuth nitrate pentahydrate

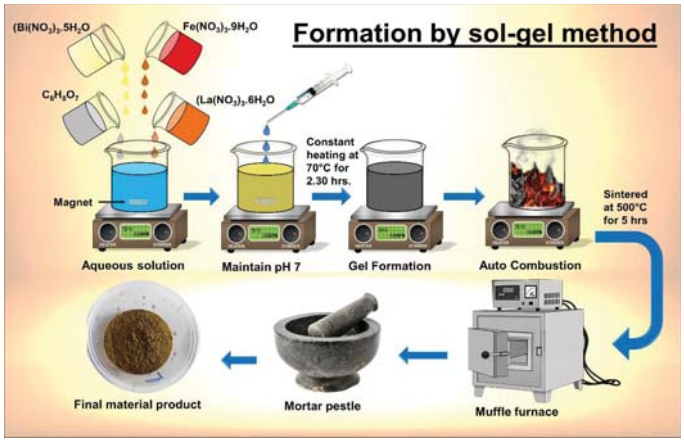

Figure 1: Schematic of the sol-gel method for the formation of $Bi_{1-x}La_xFeO_3$ thin films.

($Bi(NO_3)_3{\cdot}5H_2O$), ferric nitrate nonahydrate ($Fe(NO_3)_3{\cdot}9H_2O$), and lanthanum nitrate hexahydrate ($La(NO_3)_3{\cdot}6H_2O$) were dissolved separately in distilled water to provide the respective Bi^{3+}, Fe^{3+}, and La^{3+} ions. The precursors were mixed in a stoichiometric ratio corresponding to $Bi_{0.75}La_{0.25}FeO_3$. The combined solution was heated at 60 °C - 70 °C under constant magnetic stirring to ensure complete dissolution and homogeneity. Subsequently, aqueous ammonia was added dropwise to adjust the pH to approximately 7. This neutral pH condition facilitates controlled hydrolysis and condensation reactions, which are essential for the formation of a stable sol in the sol–gel process [7,9]. The mixture was further stirred for about 2.5 hours at the same temperature.

The solution gradually transformed into a viscous sol, indicating the progression of gelation. Additional stirring for 1 hour enhanced the uniformity and stability of the sol. The obtained sol was then subjected to an auto-combustion process, where the organic constituents (mainly citric acid) acted as fuel and underwent self-ignition upon heating, resulting in the formation of a porous precursor powder [6,8]. Thermal characterization of the precursor was carried out using thermo gravimetric analysis (TGA) and differential thermal analysis (DTA) to determine the decomposition behavior and suitable calcination temperature [10]. Based on these analyses, the as-burnt powder was calcined at 500 °C for 5 hours to obtain well-crystallized $Bi_{0.75}La_{0.25}FeO_3$ nanopowders. The $Bi_{0.75}La_{0.25}FeO_3$ powder was used to make thick films for the gas sensing measurements. The glass substrates were cleaned by soaking them in a chromic acid solution (2 g in 30 ml of double-distilled water) for 10 minutes, and then the substrates were left to soak in the solution overnight. The substrates were then washed thoroughly with ethanol and double-distilled water and dried in an oven. The powder was mixed with ethyl cellulose in the ratio 100:10 using an agate mortar, and then turpentine oil was added dropwise to the mixture to make the desired slurry. The mixture was then coated onto the cleaned glass substrates using the brush coating method, and the coated substrates were dried in the furnace at 250 °C for 15 minutes.

The performance of the fabricated sensor in the detection of the target gas was evaluated in terms of the percentage response of the sensor. The sensor response ((S%)) in the presence of the target gas was determined in terms of the change in the electrical resistance of the sensor, as indicated in the following expression:

$$s(\%) = \frac{R_{gas} - R_{air}}{R_{air}} \times 100$$

In the case of the sensor response in the presence of the reducing gases, the expression can be

$$s(\%) = \frac{R_{air} - R_{gas}}{R_{air}} \times 100$$

The expression ensures the sensor response is always positive, which enables the performance of the sensor in the presence of different concentrations of the target gases to be compared effectively. The synthesized sample was subsequently used for structural, morphological, and gas-sensing studies to evaluate its suitability for sensing applications.

Results and discussion

Structural and elemental characterizations

The phase purity and crystal structure of the synthesized $Bi_{0.75}La_{0.25}FeO_3$ nanopowders were examined using X-ray diffraction in the 2θ range of 10°-75°, as shown in Figure 2. The diffraction pattern exhibits well-defined and sharp peaks, indicating the formation of a highly crystalline material. The observed diffraction peaks were indexed to the rhombohedral perovskite structure with space group *R3c*, which is characteristic of $BiFeO_3$ -based compounds. Prominent reflections corresponding to the crystallographic planes such as (012), (104), (110), (006), (202), (224), (116), (122), (018), and (214) were clearly identified. The strong and sharp peak near 2θ ≈ 32° corresponding to the (104)/(110) planes confirms the formation of the perovskite phase and is consistent with previously reported results [11,12]. No significant impurity peaks related to secondary phases were detected within the resolution limit of the instrument, suggesting that lanthanum substitution does not disturb the primary crystal structure but rather stabilizes the perovskite phase. The slight shifting of diffraction peaks compared to pure $BiFeO_3$ can be attributed to the substitution of Bi^{3+} ions (ionic radius ~1.17 Å) with smaller La^{3+} ions (~1.16 Å), leading to lattice distortion and modification in lattice parameters [13]. The broadening of diffraction peaks indicates the nanocrystalline nature of the synthesized material. This broadening is generally associated with reduced crystallite size and possible microstrain within the lattice. The incorporation of La^{3+} ions is known to inhibit grain growth and enhance nucleation during the synthesis process, resulting in finer crystallites [14]. Furthermore, the relative intensity of peaks suggests good crystallinity and preferred orientation along specific planes, which may influence the surface-related properties such as gas adsorption and sensing performance. The improved structural stability and reduced defect concentration due to lanthanum doping are expected to enhance the functional properties of the material, particularly in gas-sensing applications [15].

The functional groups and bonding characteristics of the synthesized $Bi_{0.75}La_{0.25}FeO_3$ nanopowders were investigated using Fourier transform infrared (FTIR) spectroscopy in the wavenumber range of 4000–500 cm^{-1}, as shown in Figure 3. The FTIR spectrum exhibits several characteristic absorption bands corresponding to different vibrational modes present in the material. A weak absorption band observed around 2990 cm^{-1} can be attributed to the stretching vibrations of residual C–H bonds, which may arise from the incomplete decomposition of organic precursors such as citric acid used during the sol–gel auto-combustion process [16]. The band near 2360 cm^{-1} is commonly associated with the presence of atmospheric CO_2 or asymmetric stretching vibrations of carbonyl groups. A prominent absorption band around 1060 cm^{-1} is assigned to C–O stretching or metal–oxygen bonding interactions, indicating the presence of residual organic moieties or intermediate compounds formed during synthesis. The presence of such bands suggests that trace amounts of organic species may still be present after calcination, although significantly reduced [16,17]. The most significant feature of the FTIR spectrum is the strong absorption band observed at approximately 532 cm^{-1}, which is attributed to the Fe-O stretching vibration within the FeO_6 octahedral units of the perovskite structure. This band is a characteristic signature of

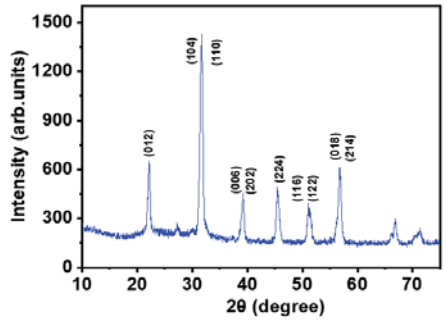

Figure 2: The XRD patterns of $Bi_{0.75}La_{0.25}FeO_3$ nanopowders.

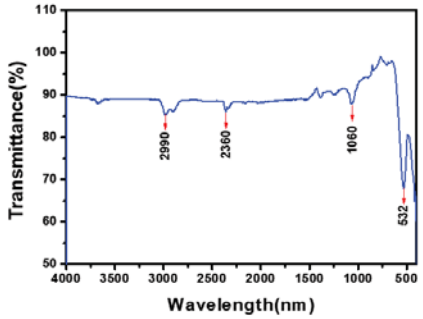

Figure 3: FTIR spectra of $Bi_{0.75}La_{0.25}FeO_3$ nanopowders.

$BiFeO_3$-based materials and confirms the successful formation of the perovskite phase [17]. The position and intensity of this band also indicate that the incorporation of La^{3+} ions does not disrupt the fundamental Fe–O bonding network but may induce slight lattice distortions. Overall, the FTIR analysis supports the formation of lanthanum-doped bismuth ferrite with a well-defined perovskite structure. The presence of characteristic Fe-O vibrations along with minimal residual organic peaks confirms the effectiveness of the synthesis and calcination processes.

The surface morphology and microstructural features of the synthesized $Bi_{0.75}La_{0.25}FeO_3$ nanopowders were examined using field emission scanning electron microscopy (FESEM), as shown in Figure 4(A and B). The low-magnification image (25KX) in Figure 4(A) reveals that the sample consists of densely packed agglomerates with irregular morphology. These agglomerates are formed due to the high surface energy of nanoparticles, which promotes particle clustering during the synthesis and subsequent calcination process. The surface appears relatively porous, which is beneficial for gas-sensing applications as it provides a larger active surface area for gas adsorption [18]. The high-magnification image (100KX) in Figure 4(B) provides a clearer view of the nanoscale features, showing that the material is composed of nearly spherical to spherical nanoparticles with a relatively uniform size distribution. The particles are interconnected, forming a network-like structure with grain boundaries clearly visible. The estimated particle size lies in the nanometer range, which is consistent with the peak broadening observed in the XRD analysis. The reduction in particle size can be attributed to the presence of La^{3+} ions, which inhibit grain growth and promote nucleation during the synthesis process [19]. Additionally, the presence of slight agglomeration is typical for sol–gel derived nanopowders due to the combustion process, where rapid release of gases leads to the formation of loosely bound clusters. Despite this agglomeration, the material maintains a porous and rough surface morphology, which is advantageous for enhancing gas diffusion and surface reactions in sensing applications [20]. Overall, the FESEM analysis confirms the formation of nanosized, agglomerated particles with a porous morphology. Such structural characteristics are highly favorable for gas-sensing performance, as they facilitate efficient adsorption and interaction of gas molecules with the sensing surface.

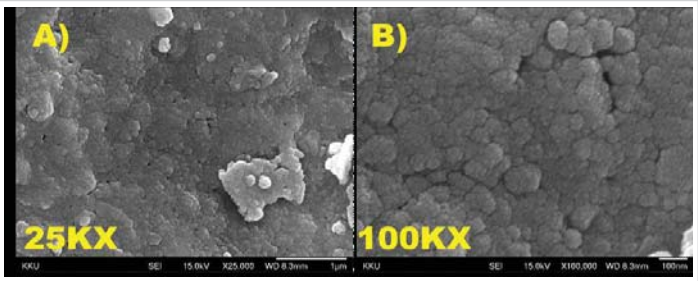

Figure 4: The SEM images of A) $Bi_{0.75}La_{0.25}FeO_3$ nanopowders at 25KX and, B) 100KX magnifications, respectively.

Gas sensing result and analysis

The gas-sensing characteristics of the synthesized $Bi_{0.75}La_{0.25}FeO_3$ nanopowders were systematically evaluated toward different target gases, including NO_2, CO_2, ethanol, and NH_3, at an optimized operating temperature of 200 °C. As shown in Figure 5(A), the experimental setup of the gas sensing system is presented to analyze the powder material of the La-doped $BiFeO_3$. In the experiment, the gas response characteristics can be precisely measured using the La-doped bismuth ferrite samples. All the data analysis was conducted on the La-doped $BiFeO_3$ powder to analyze the sensing performance of the material. Figure 5(B) illustrates the selectivity of the sensor toward various gases. The material exhibits a significantly higher response toward NH_3 (82%) compared to ethanol (25%), CO_2 (15%), and NO_2 (5%). This indicates that the La-doped $BiFeO_3$ sensor possesses excellent selectivity toward ammonia gas. The enhanced selectivity can be attributed to the strong interaction between NH_3 molecules and the adsorbed oxygen species on the sensor surface, as well as the increased surface activity induced by lanthanum doping [21,22]. The dynamic response time of 11 s and recovery time of 64 s of the sensor toward NH_3 is presented in Figure 5(C). Upon exposure to NH_3 gas, the sensor resistance decreases sharply, indicating typical p-type semiconducting behavior of $BiFeO_3$. This decrease in resistance is due to the reaction of reducing NH_3 gas with adsorbed oxygen species (O_2^-, O^-), which releases electrons back to the conduction band and reduces hole concentration [23]. The sensor exhibits a rapid response followed by a gradual recovery when the gas is removed, demonstrating good reversibility and stability. Figure 5(D) shows the transient response curve, highlighting the response and recovery times of the sensor. The response time (time required to reach 90% of the total resistance change) is relatively short, indicating fast adsorption kinetics of NH_3 molecules. Similarly, the recovery time is moderate, suggesting efficient desorption of gas molecules from the surface. The slight delay in recovery may be attributed to strong adsorption of NH_3 on active sites, which is beneficial for achieving high sensitivity [24]. The improved sensing performance of La-doped $BiFeO_3$ can be explained by several factors. Firstly, lanthanum substitution enhances oxygen vacancy concentration, which increases the number of active sites available for gas adsorption. Secondly, the nanoscale particle size and porous morphology, as confirmed by SEM analysis, provide a high surface-to-volume ratio, facilitating efficient gas diffusion and interaction. Lastly, the modification in electronic structure due to La doping improves charge transfer processes, thereby enhancing sensor response [22,25].

The dynamic gas-sensing behavior of La-doped $BiFeO_3$ nanopowders toward NH_3 gas at different concentrations (10–100 ppm) was investigated, as illustrated in Figure 5(E). The sensor exhibits a clear and repeatable change in resistance upon exposure to NH_3, demonstrating good reproducibility

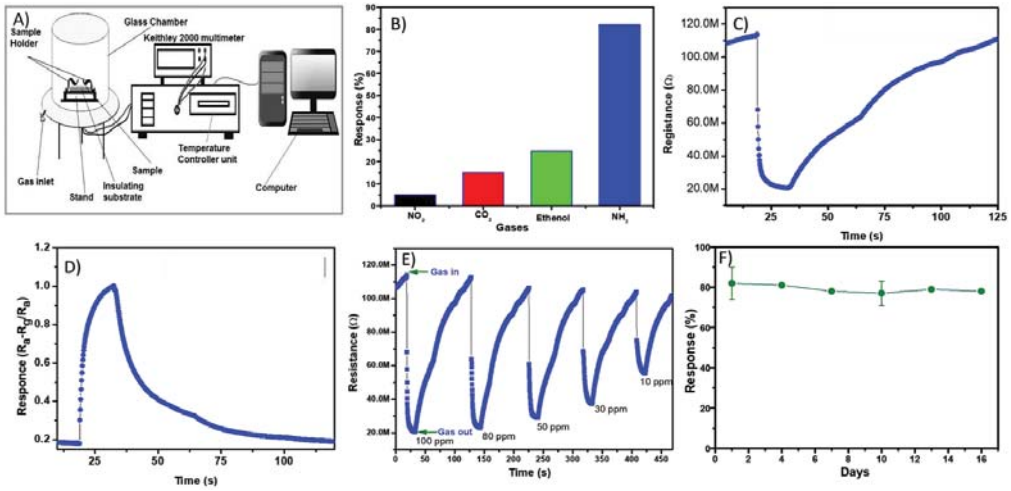

Figure 5: A) Gas sensing system. B) Selectivity of the prepared sensor towards different test gases. C, D) La-doped $BiFeO_3$ ($Bi_{0.75}La_{0.25}FeO_3$) sensor Resistance *vs.* time curve. E) Sensitivity curve of La-doped $BiFeO_3$ sensor at different ppm. F) long-term stability of La-doped $BiFeO_3$ sensor.

Table 1

Sr. No.	Material / Sensor	Target Gas	Sensitivity / Response	Response Time and Recovery Time (s)	Operating Temp (°C)	Reference
	La-doped $BiFeO_3$ thin films	Co	High (enhanced *vs.* pure BFO)	0.40/0.60	Room Temp. Moderate	[28]
	Pure $BiFeO_3$ (BFO)	Co	Moderate	0.91/1.2	Moderate	[29]
	Ca-doped $BiFeO_3$	H_2	High (~212% at 500 ppm)	20/40	225 °C - 2 50 °C	[30]
	Sr-doped $BiFeO_3$	Acetone/Ethanol	Improved over pure BFO	15/30	~208 °C (reduced from 244 °C)	[31]
	Er-doped $BiFeO_3$	Acetone	High sensitivity (enhanced via doping)	18/35	~200 - 300 °C	[32]
	La-doped $BiFeO_3$ ($Bi_{0.75}La_{0.25}FeO_3$)	NH_3	High sensitivity (enhanced via doping)	11/64	200	Present work

and reliability. It is observed that the magnitude of resistance change increases with increasing NH_3 concentration, from 10 ppm to 100 ppm. At higher concentrations, a more pronounced drop in resistance is recorded, indicating a higher sensor response. This behavior can be attributed to the increased interaction between NH_3 molecules and adsorbed oxygen species on the sensor surface, leading to enhanced electron transfer and modulation of charge carriers [26]. The response and recovery cycles are consistent across multiple exposures, indicating good repeatability of the sensing material. The response curve also reveals that the sensor exhibits relatively fast response and moderate recovery times across all tested concentrations. The gradual recovery behavior suggests strong adsorption of NH_3 molecules on the active surface sites, which is beneficial for achieving high sensitivity. Additionally, the porous nanostructure observed in SEM analysis facilitates efficient gas diffusion, contributing to improved sensing performance. Figure 5(F) presents the stability of the sensor over a period of 16 days. The sensor response remains nearly constant (~78% - 82%) throughout the testing duration, with only minor fluctuations. This indicates excellent long-term stability and reliability of the La-doped $BiFeO_3$ sensor. The slight variation in response may be attributed to environmental factors such as humidity and temperature, but the overall performance remains consistent. The stability of the sensor can be attributed to the structural robustness of the perovskite phase and the enhanced chemical stability imparted by lanthanum doping [27]. Overall, the results demonstrate that the La-doped $BiFeO_3$ nanopowders exhibit strong concentration-dependent sensing behavior, good repeatability, and excellent long-term stability, making them highly suitable for practical NH_3 gas sensing applications (Table 1 above).

Conclusions

The $Bi_{0.75}La_{0.25}FeO_3$ nanopowders were successfully synthesized via a sol–gel auto-combustion method. XRD and FTIR analyses confirmed the formation of a rhombohedral perovskite structure, while FESEM revealed a nanosized and porous morphology favorable for gas sensing. The material exhibited high selectivity and strong response (~82%) toward NH_3 at 200 °C, along with good repeatability and stability. The enhanced performance is attributed to La-induced oxygen vacancies, reduced particle size, and increased surface activity, which facilitate efficient gas adsorption and charge transfer. Additionally, the sensor demonstrated a clear concentration-dependent response in the range of 10–100 ppm and maintained stable performance over extended periods, indicating good reliability. The combination of structural stability, improved surface properties, and excellent sensing characteristics highlights the potential of La-doped $BiFeO_3$ as an effective material for practical NH_3 gas sensing applications.

Acknowledgement

The authors would like to thank and acknowledge the Chhatrapati Shahu Maharaj Research Training and Human Development Institute (SARTHI), Pune, Government of Maharashtra, India, and the 'Seed money project' in academic year 2025-26 of Vivekanand College, Kolhapur (An Empowered Autonomous Institute) for funding support.

References

1. Ghadage P, Shinde KP, Nadargi D, Nadargi J, Shaikh H, Alam MA, et al. Bismuth ferrite-based acetone gas sensor: evaluation of graphene oxide loading. RSC Adv. 2024;14:1367–1376. Available from: https://pubs.rsc.org/en/content/articlelanding/2024/ra/d3ra06733e
2. Shetty C, Shastrimath VVD. Pure and barium-substituted bismuth ferrite as an ethanol gas sensor. Surf Interfaces. 2024;46:103942. Available from: https://doi.org/10.1016/j.surfin.2024.103942
3. Zhang X. Indium-doped BiFeO3 gas sensors for high-sensitivity SO2F2 detection. J Adv Compos Mater. 2024. Available from: https://doi.org/10.1016/j.jacomc.2024.100021
4. Zhao Y, Zhang X, Wang M, Meng L, Wang M, Hussain S, et al. La-doped mullite $Bi2Fe_4O_9$ chemiresistive gas sensor for ultra-highly selective detection of ethylene glycol. Adv Mater. 2026;38(10):e17585. Available from: https://doi.org/10.1002/adma.202517585
5. Sumayli A, Alamoudi JA, Alqahtani AS. A superior ethylene glycol gas sensor based on cobalt doped highly porous $ZnFe_2O_4$ microspheres. Sci Rep. 2025;15(1):23168. Available from: https://doi.org/10.1038/s41598-025-04481-8
6. Patil DR, Lokhande CD. Auto-combustion synthesis of nanostructured metal oxides for gas sensing applications. Mater Chem Phys. 2021;271:124911.
7. Sharma P, Gupta R. Sol–gel synthesis and characterization of perovskite oxide nanomaterials. J Sol-Gel Sci Technol. 2022;101(2):456–468.
8. Singh S. Role of citric acid in sol–gel auto-combustion synthesis of nanomaterials. Ceram Int. 2023;49(5):7421–7430.
9. Kumar A, Yadav KL. Effect of pH on structural and electrical properties of $BiFeO_3$ nanoparticles. J Mater Sci Mater Electron. 2021;32:11234–11242.
10. Zhang Y. Thermal analysis and phase evolution of perovskite oxide nanomaterials. Thermochim Acta. 2024;726:179245.
11. Wang J. Structural and magnetic properties of $BiFeO_3$ nanoparticles. J Alloys Compd. 2021;861:158564.
12. Kumar M. Effect of rare-earth doping on structural properties of $BiFeO_3$. Ceram Int. 2022;48(3):3456–3464.
13. Singh A. Influence of La substitution on lattice distortion in $BiFeO_3$. Mater Lett. 2023;330:133198.
14. Zhao L. Size-dependent structural and optical properties of $BiFeO_3$ nanoparticles. Appl Phys A. 2021;127:112.
15. Chen X. Enhanced gas sensing performance of doped perovskite oxides. Sens Actuators B Chem. 2024;405:135341.
16. Kumar A. FTIR and structural analysis of $BiFeO_3$-based perovskite nanomaterials. J Mater Sci Mater Electron. 2022;33:15432–15440.
17. Zhang L. Morphological control of nanostructured metal oxides for gas sensing applications. Sens Actuators B Chem. 2021;345:130371.
18. Kumar R. Effect of rare-earth doping on microstructure and properties of $BiFeO_3$ nanoparticles. Ceram Int. 2022;48(7):9876–9884.
19. Singh P. Influence of synthesis method on morphology and gas sensing behavior of perovskite nanomaterials. Appl Surf Sci. 2023;612:155876.
20. Zhang T. Recent advances in metal oxide gas sensors: sensitivity and selectivity. Sens Actuators B Chem. 2021;330:129333.
21. Kumar R. Enhanced ammonia sensing performance of doped perovskite oxides. Ceram Int. 2022;48(10):14567–14575.
22. Wang C, Yin L, Zhang L, Xiang D, Gao R. Metal oxide gas sensors: sensitivity and influencing factors. Sensors. 2010;10(3):2088–2106. Available from: https://doi.org/10.3390/s100302088
23. Singh P. Response and recovery characteristics of nanostructured gas sensors. Appl Surf Sci. 2023;615:156321.
24. Chen X. Role of oxygen vacancies in enhancing gas sensing performance. J Mater Chem C. 2024;12:5678–5687.
25. Zhang T. Stability and repeatability of semiconductor gas sensors. Sens Actuators B Chem. 2022;357:131415.
26. Dey A. Semiconductor metal oxide gas sensors: a review. Mater Sci Eng B. 2018;229:206–217. Available from: https://doi.org/10.1016/j.mseb.2017.12.036
27. Barsan N, Weimar U. Conduction model of metal oxide gas sensors. J Electroceram. 2001;7:143–167. Available from: https://link.springer.com/article/10.1023/A:1014405811371
28. Pinto JV, Fernandes MM, Costa FM. Enhanced carbon monoxide sensing performance of La-doped $BiFeO_3$ thin films. Ceram Int. 2025.
29. Pinto JV, Fernandes MM, Costa FM. Gas sensing characteristics of pure $BiFeO_3$ thin films for CO detection. Ceram Int. 2025.
30. Bala R, Singh R, Sharma A. Hydrogen sensing properties of Ca-doped $BiFeO_3$ nanostructures. Int J Hydrogen Energy. 2019.
31. Zhang L, Wang Y, Liu X. Improved acetone sensing performance of Sr-doped $BiFeO_3$ nanoparticles. J Adv Ceram. 2022.
32. Liu H, Chen Y, Zhao Q. Enhanced acetone gas sensing properties of Er-doped $BiFeO_3$ nanomaterials. Mater Lett. 2022.